Quaternary Geochronology 54 (2019) 101008

Contents lists available at ScienceDirect

Quaternary Geochronology

journal homepage: www.elsevier.com/locate/quageo

Detecting landscape transience with in situ cosmogenic ^{14}C and ^{10}Be

Daniel S. Skov[a,*], David L. Egholm[a], John D. Jansen[a], Mike Sandiford[b], Mads F. Knudsen[a]

[a] Department of Geoscience, Aarhus University, Høegh-Guldbergsgade 2, 8000 Aarhus C, Denmark
[b] School of Earth Sciences, University of Melbourne, 253-283 Elgin St, Carlton, VIC 3053, Australia

A B S T R A C T

Constraining past variations in rates of erosion remains a key challenge in geomorphology, as estimates of erosion rate on different timescales must be bridged. The Late Pleistocene to Holocene represents a key timescale for studying landscape transience, as climatic change, increasing anthropogenic activity, and/or tectonic activity changed the rate of surface processes in many landscapes. Few chronometers are suitable for studying surface processes and landscape transience on these timescales, but, although not yet widely used, in situ ^{14}C holds much promise due to its appropriate half-life of 5.7 kyr. Furthermore, by pairing in situ ^{14}C with a stable or longer-lived nuclide, such as ^{10}Be, ^{21}Ne or ^{26}Al, it is possible to compare surface process rates on distinctly different timescales. In this paper, we explore how these paired chronometers can be used to study landscape transience in non-glacial landscapes on Late Pleistocene to Holocene timescales. Indeed, we find that paired measurements of in situ ^{14}C and a long-lived cosmogenic nuclide (CN) in samples from eroding landscapes enable the detection of changes in erosion rate during the Late Pleistocene to Holocene, if the increase or decrease in erosion rate was larger than a factor of two, and the landscape is eroding at rates that are typical for fluvial landscapes (5–500 mm/kyr). Similarly, detecting changes in catchment-wide denudation rates using paired CN measurements in stream-sediment samples is also possible in catchments with suitable conditions, such as short sediment transport times, minimal erosion from deep-seated mass movement, etc. (von Blanckenburg, 2006).

1. Introduction

On geological timescales, changes in tectonic activity and fluctuations in climate have forced much of Earth's surface to continuously adjust, implying that landscape transience is ubiquitous (Whipple, 2001). During the Quaternary, large-scale climatic changes altered the rate of surface processes in many landscapes. In glacial settings, the waxing and waning of glaciers reshaped landscapes dramatically. In non-glacial landscapes, variations in vegetation cover (Roering et al., 2004), precipitation (D'Arcy et al., 2017; Ferrier et al., 2013), temperature (including frost) (Andersen et al., 2015; Hales and Roering, 2007; Marshall et al., 2015; Small et al., 1997), and human activity (Milliman and Syvitski, 1992; Montgomery, 2007; Syvitski, 2003) altered the style and rate of erosion. The erosional response to such changes likely varied in space and time, but the nature and magnitude of the response is difficult to predict (Fig. 1). For example, increasing temperatures may accelerate erosion due to more effective weathering (Hidy et al., 2014), but decreasing temperatures might also accelerate erosion, e.g. due to initiation of frost weathering and periglacial activity (Marshall et al., 2015). While some studies find that faster erosion rates correlate with higher mean-annual precipitation (Ferrier et al., 2013), others find that erosion rates do not correlate with mean-annual precipitation, but rather with the frequency of storms (D'Arcy et al., 2017). Additionally, temperature and precipitation both impact the hydrological cycle and vegetation cover (Collins, 2004; Langbein and Schumm, 1958), further complicating a prediction of the erosional response to changes in climate. Similarly, tectonic processes may also affect surface-process rates in many ways, e.g. by steepening or flattening landscapes. In recent times, human land use has radically impacted surface-process rates (Milliman and Syvitski, 1992; Montgomery, 2007; Syvitski, 2003). During the Late Pleistocene and Holocene, humans spread across the world and began to exert an ever increasing impact on the natural landscape processes through agriculture, deforestation, mining, and water management etc. (Milliman and Syvitski, 1992). Consequently, constraining past variations in erosion rate is not only essential for disentangling the natural processes controlling the evolution of landscapes, but also for identifying the human influence on surface processes.

Over the past two decades, our quantitative understanding of erosion rates has been greatly improved through the application of methods based on in situ cosmogenic nuclides (CNs) (Granger et al., 2013). Due to the strong depth-dependence of CN production, the concentration of CNs in a sample is proportional to the amount of time spent in the upper few metres beneath the landscape surface (Lal, 1991). CNs can therefore be used to quantify rates of erosion and durations of transport, and the possibility of measuring CNs in both

* Corresponding author.
E-mail addresses: daniel.skov@geo.au.dk (D.S. Skov), david@geo.au.dk (D.L. Egholm), jdj@geo.au.dk (J.D. Jansen), mikes@unimelb.edu.au (M. Sandiford), mfk@geo.au.dk (M.F. Knudsen).

https://doi.org/10.1016/j.quageo.2019.101008
Received 26 July 2018; Received in revised form 21 June 2019; Accepted 27 June 2019
Available online 29 June 2019

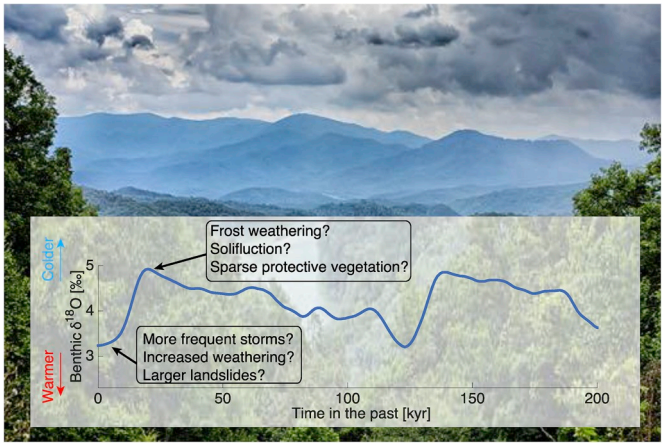

Fig. 1. The erosion rate in fluvial landscapes vary trough time, e.g. in response to changes in tectonics, climate or anthropogenic factors. The effect of a change in boundary conditions on erosion rate are not always straightforward, e.g. increasing precipitation might both increase erosion rates via faster river incision, but may also decrease erosion rates due to more widespread vegetative cover.

erosional and depositional settings adds much versatility. The CN concentration in a sample represents a time-integrated measure of the erosion and exposure history, and the CN concentration in bedrock and sediment samples from hillslopes, as well as in stream-sediment samples, can be interpreted as an apparent erosion rate (Granger et al., 1996; Lal, 1991). Several studies have utilized erosion rates estimated from a single CN to study past variations in erosion rates, e.g. by comparing ^{10}Be erosion rates to present-day river sediment loads (Schaller et al., 2001), or by estimating paleo-denudation rates using time series of ^{10}Be erosion rates from independently dated sedimentary archives (Charreau et al., 2011; Garcin et al., 2017; Grischott et al., 2017; Marshall et al., 2015; Schaller and Ehlers, 2006).Another approach to study past variations in erosion rates is to estimate erosion rates using multiple CNs in a single sample. The length of "memory" integrated in a measured CN concentration varies for different erosion rates and lengths of radioactive half-life. Thus, measurement of multiple CNs makes it possible to compare surface-process rates on different timescales, and possibly detect past landscape transience (Lal, 1991; Mudd, 2017). However, the half-lives of the most commonly measured nuclides, ^{10}Be and ^{26}Al (~1.4 Myr and 0.7 Myr, respectively), are both much longer than the Holocene and Late Pleistocene, and this pair of nuclides is therefore unsuited to study transience on these timescales (Mudd, 2017). In contrast, when paired with ^{10}Be or ^{26}Al, in situ ^{14}C is uniquely suited for the Late Pleistocene to Holocene timescales due to the short half-life of ~5.7 kyr. Indeed, although not yet widely used, several studies have shown that landscape transience on millennial timescales can be studied using paired measurements of in situ ^{14}C and a long-lived CN (Fülöp et al., 2015; Hippe, 2017; Hippe et al., 2012; Mudd, 2017). Hippe (2017) and Mudd (2017) showed that paired ^{14}C-^{10}Be from a hillslope sample can be used to detect landscape transience, but that the magnitude and timing of the change in erosion rate cannot be constrained, not even using a depth profile. This is, however, possible in sedimentary deposits of known age, as shown by (Fülöp et al., 2015), who used a depth profile of in situ cosmogenic ^{10}Be and ^{14}C concentrations in a moraine to quantify the magnitude and timing of a post-depositional erosional event. In general, the use of paired in situ CNs to detect landscape transience has several advantages. First, erosion rates estimated using CNs in hillslope samples represent direct quantification of the surface processes at the site, and thus do not require corrections for sediment transport and storage or source-to-sink coupling that may obscure the landscape transience otherwise embedded in the CN signal (Jerolmack and Paola, 2010). Second, paired CNs can be studied in landscapes where sedimentary archives are sparse. Paired measurements of CNs can also be used to quantify catchment-wide changes in erosion rate, but the concentration of in situ ^{14}C in stream-sediment samples is highly sensitive to other processes than erosion, such as radioactive decay during transport and/or soil-mixing on hillslopes (Hippe, 2017; Hippe et al., 2012; von Blanckenburg, 2006). The method is therefore not applicable to catchments characterized by slow erosion rates, deep mixing, significant sediment storage, etc. (see von Blanckenburg (2006) for a full discussion).

In this paper, we expand upon the results of Hippe (2017) and Mudd (2017) by mapping when and how paired measurements of in situ ^{14}C and ^{10}Be can be used to detect landscape transience. Additionally, in contrast to previous studies, we discuss the implications of a) non-linear uncertainties associated with estimating apparent erosion rates, and b) the importance of production by muons, either of which can be of great importance in both slowly eroding and rapidly eroding landscapes. Moreover, we outline three plausible models of Late Pleistocene to Holocene erosion as useful test scenarios for exploring how landscape transience on these timescales can be detected using paired measurements of in situ ^{14}C and ^{10}Be in hillslope or stream-sediment samples.

2. Methods

Our strategy is to 1) assume a transient history of erosion rate and from that calculate nuclide concentrations of synthetic samples, 2) add uncertainties to the calculated nuclide concentrations to reflect uncertainties of real nuclide measurements, 3) 'inverse model' the synthetic nuclide concentrations by comparing steady-state 'apparent' erosion rates derived from different CNs. If these steady-state erosion rates differ, we know that one or more of the nuclide concentrations are not in a steady state, and that the erosion rate has changed. From this information we can explore under what settings a pair of two different CNs can resolve the timing and magnitude of the change.

The CN concentration, N, resulting from any given exhumation history can be calculated by integrating the production and removal of nuclides over time:

$$\frac{dN}{dt} = P(z,t) - \lambda N(z,t) \quad (1)$$

with

$$z(t) = \int_0^t \varepsilon(t)dt \quad (2)$$

Here P(z,t) is the nuclide production rate at depth z and time t; λ is the decay constant; $\varepsilon(t)$ is rate of erosion. Hence, in continuously exposed landscapes, the CN concentration is only a function of the exhumation history, and thus past erosion rates. However, the CN concentration resulting from a given exhumation history is inherently non-unique, as different exhumation histories can result in the same CN concentration, or pair of CN concentrations (Knudsen and Egholm, 2018). The full erosion history, $\varepsilon(t)$, can therefore not generally be determined by inverse modelling the measured CN concentrations.

Cosmic-ray bombardment of the Earth's surface results in production of a variety of CNs in rocks and soils, primarily within a few metres of the surface. CN production occurs via a number of processes, including spallation, negative muon capture, and deceleration of fast muons (Heisinger et al., 2002b, 2002a; Lal, 1991). For many commonly measured CNs, e.g. ^{10}Be, ^{26}Al, and ^{14}C in quartz, the rates of production and radioactive decay are relatively well constrained (Balco, 2017; Balco et al., 2008; Borchers et al., 2016; Heisinger et al., 2002b, 2002a; Lupker et al., 2015; Marrero et al., 2016; Phillips et al., 2016), which makes it possible to extract information about landscape histories on 10^2–10^6 year timescales.

The spallogenic production rate of CNs follows a well-established

Table 1
List of parameters used in the models.

Parameters	Symbol	Value	References/notes
Decay constant ^{10}Be	λ_{Be}	ln(2)/1.387E6 yr	(Chmeleff et al., 2010; Korschinek et al., 2010)
Decay constant ^{14}C	λ_{C}	ln(2)/5700 yr	
Decay constant ^{26}Al	λ_{Al}	ln(2)/0.705E6 yr	Nishiizumi (2004)
Attenuation length for spallation	Λ_{sp}	160 g cm^{-2}	(Balco et al., 2008; Gosse and Phillips, 2001)
Reference cross-section at 1 GeV	σ_0	^{10}Be: 0.280μb	(Balco, 2017) model 1A, $\alpha = 1$
		^{26}Al: 3.89 μb	Heisinger et al. (2002b)
		^{14}C: 2.39 μb	
Negative muon capture probability	f*	^{10}Be: 0.191%	(Balco, 2017) model 1A, $\alpha = 1$
		^{26}Al: 1.33%	Heisinger et al. (2002a)
		^{14}C: 13.7%	
Number of target nuclei per gram quartz	N	^{10}Be: 2.006E22 atoms g^{-1}	
		^{26}Al: 1.003E22 atoms g^{-1}	
		^{14}C: 2.006E22 atoms g^{-1}	
Density	ρ	2.6 g cm^{-3}	
Surface production rate of nuclide due to spallation	$P(0)_{spal}$	^{10}Be: 4.01 atoms g^{-1} yr^{-1}	(Borchers et al., 2016; Phillips et al., 2016)
		^{26}Al: 27.93 atoms g^{-1} yr^{-1}	
		^{14}C: 12.24 atoms g^{-1} yr^{-1}	

exponential decrease with depth (Gosse and Phillips, 2001; Marrero et al., 2016). Spallation is the dominant production mechanism in the upper few meters, while production by muons dominates below this depth. The muogenic production rate scales with the muon flux and energy of the muons (Heisinger et al., 2002b, 2002a). In this paper, we calculate the muogenic production rates using the formulations from Heisinger et al. (2002b, 2002a), with updated production rate parameters for ^{10}Be and ^{26}Al from Balco (2017, model 1A, $\alpha = 1$). We use the parameters for muogenic production of in situ ^{14}C from Heisinger et al. (2002b, 2002a), as these are consistent with values based on geological calibrations (Lupker et al., 2015). All constants used in this paper are listed in Table 1. To drastically speed up calculations, we fit the total muogenic production rate with the sum of two exponential functions. We find that the best-fitting sum of two exponential functions approximates the production rates sufficiently well (less than 2% deviation down to a depth of 30 m) to not significantly affect the conclusions of this study. At Sea-level and high-latitude (SLHL) the two fitted exponential functions have e-folding lengths of ~6772 g cm^{-2} and ~1253 g cm^{-2} for ^{10}Be and ^{26}Al, and 5021 g cm^{-2} and 1162 g cm^{-2} for ^{14}C. These values differ from the more commonly used attenuation lengths of ~4200 g cm^{-2} and ~1500 g cm^{-2}, but using the these values instead would not affect the conclusions of this study.

2.1. Apparent erosion rate from CN concentrations

The *apparent* erosion rate ε_{app} [m/yr] is a frequently used measure to represent CN concentrations. ε_{app} is the constant erosion rate corresponding to a specific steady-state CN concentration. Estimating apparent erosion rates from CN concentration is a bounding model, the opposing bounding model being no erosion and a finite exposure age. Estimates of apparent erosion are thus only valid in steadily eroding landscapes where the CN concentrations have not been influenced by periods of burial, or any other process besides steady erosion. We use apparent erosion rates calculated for different CNs to check for steady-state conditions. If the apparent erosion rates of two different CNs differ, we know that the steady-state conditions have been violated and that erosion rates may have changed in time.

By approximating the depth-dependence of production rates with a set of exponential functions, the steady-state CN concentration can be calculated as

$$C_{i,d,SS} = \sum_{j=1}^{n} \left[\frac{P_{0,i,j}}{\lambda_i + \varepsilon_{app}\rho/\Lambda_j} e^{-d\rho/\Lambda_j} \right] \quad (3)$$

where $C_{i,t,SS}$ [atoms kg^{-1}] is the steady-state concentration of nuclide i at depth d [m], λ_i [yr^{-1}] is the decay constant of nuclide i, $P_{0,i,j}$ [atoms kg^{-1} yr^{-1}] is the production rate of nuclide i due to production mechanism j at the surface, Λ_j [kg m^{-2}] is the attenuation length of the production mechanism j, ε_{app} [m yr^{-1}] is the erosion rate, and ρ [kg m^{-3}] is the density.

For a sample at the surface, this further reduces to

$$C_{i,0,SS} = \sum_{j=1}^{n} \left[\frac{P_{0,i,j}}{\lambda_i + \varepsilon_{app}\rho/\Lambda_j} \right]. \quad (4)$$

An apparent erosion rate can thus be estimated by measuring the concentration of a specific CN and solving Eq. (4) for ε_{app} (Fig. 2). As the CN concentration in the landscape surface is a time-integrated function of the exhumation history, apparent erosion rates reflect the time-integrated variable erosion rate. Changes in apparent erosion rate therefore lag changes in actual erosion rates, and the amount of lag depends on the erosion rates and the half-life of the nuclide. Differences between estimates of apparent erosion rate based on nuclides with different half-lives therefore indicate that a change in erosion rate occurred in the past. Many previous studies have focused on the accuracy of apparent erosion rates relative to actual erosion rates (e.g. Niemi

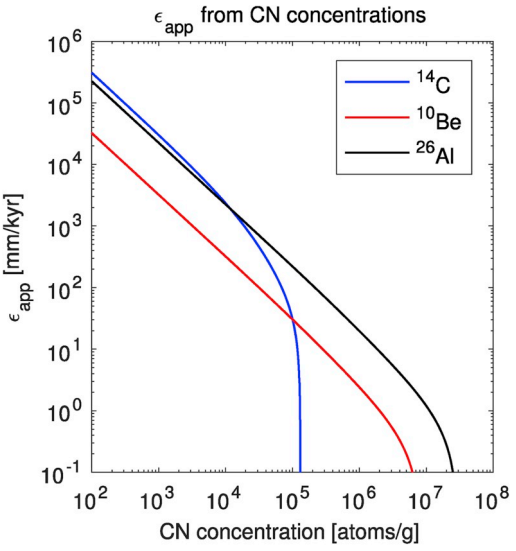

Fig. 2. The apparent erosion rate calculated from concentrations of different nuclides. In situ ^{14}C is only weakly sensitive to erosion rates between ~50 and 100 mm/kyr, and not sensitive to erosion rates below 10 mm/kyr. The longer lived and stable nuclides can resolve even very slow (> 1 mm/kyr) erosion rates reasonably well. Calculated for SLHL production rates.

et al., 2005; Yanites et al., 2009), but the possibility of using the difference between apparent erosion rates derived from CNs with different half-lives to detect past changes in erosion rates has only recently been explored (Mudd, 2017).

2.1.1. Applicability to soil-mantled landscapes and catchment-wide denudation rates

Estimation of erosion rates is more complicated in soil-mantled landscapes than in bedrock landscapes, as vertical mixing of soils, chemical erosion, and selective weathering can influence the CN concentrations (Dixon and Riebe, 2014; Granger and Riebe, 2013), and erosion rates estimated for soils might therefore not reflect actual erosion rates. Furthermore, such processes do not influence the concentration of different CNs to the same degree. For example, soil mixing to a depth of 50 cm in a landscape eroding at 50 mm/kyr lowers the in situ ^{14}C concentration in the soil surface by 10% compared to unmixed soils, while the ^{10}Be concentration is lowered by less than 1% (Hippe, 2017). For landscapes with deeper mixing, and/or slower erosion rates, the in situ ^{14}C content in a surface sample would be even lower (Hippe, 2017). The effect of such processes must thus be accounted for when trying to estimate landscape transience in soil-mantled landscapes.

Measurement of CNs in stream-sediment samples can also be used to estimate apparent catchment-wide denudation rates (Bierman and Steig, 1996; Brown et al., 1995; Granger et al., 1996). Estimated catchment-wide erosion rates are only accurate under suitable circumstances (von Blanckenburg, 2006), including: 1) uniform erosion rates in time and space, 2) similar grain-size distributions released across the catchment, and 3) short durations of sediment storage and transport relative to the radioactive half-life of the CN. In catchments where the timescale associated with sediment storage and transport is not significantly shorter than the timescale of the radioactive decay, catchment-wide denudation rates estimated in this way only represent maximum-limiting rates. Due to its relatively long half-life, ^{10}Be is less sensitive to these effects than nuclides with shorter half-lives, such as ^{14}C, and measurements of ^{10}Be in stream-sediment samples are routinely used to estimate catchment-wide denudation rates (e.g. Schaller et al., 2002). Estimating catchment-wide denudations rates using the in situ ^{14}C concentration in stream-sediment samples is, however, less robust. Variable rates of erosion across the landscape, soil-mixing processes, deep-seated mass-removal, and temporary sediment storage influence the in situ ^{14}C concentration to a much larger degree than the ^{10}Be concentration (Hippe et al., 2012; von Blanckenburg, 2006). For instance, a 900-yr period of burial without production of additional nuclides lowers the ^{14}C concentration by more than 10%, whereas the ^{10}Be concentration decreases by less than 0.05%. Burial thus lowers the in situ ^{14}C concentration relative to the ^{10}Be concentration, which may result in erroneous interpretations of the past erosion history if unaccounted for. It is thus critical to recognize if soil mixing, sediment storage, mass wasting, etc., occur in the landscape before using paired measurements of in situ ^{10}Be and ^{14}C in stream samples to study the erosion history. The results presented in this study concerning catchment-wide denudation rates are only valid for landscapes characterized by spatially homogeneous erosion rates with shallow soil mixing, short periods of sediment transport and storage, and limited deep-seated mass removal etc.

2.2. Detecting changes in erosion rate using multiple CNs

If the ^{10}Be and ^{14}C concentrations from a single sample indicate statistically significant differences in apparent erosion rates, the sample experienced a complex exhumation history. The possibility that the sample experienced a complex exhumation history cannot be rejected even if the apparent erosion rates estimated using in situ ^{10}Be and ^{14}C are not statistically different, as fluctuating erosion rates might result in similar apparent erosion-rate estimates for different nuclides (Knudsen and Egholm, 2018). Additionally, the absolute difference in apparent erosion rate from different nuclides is not unique for specific exhumation histories, and the ratio between apparent erosion rates can therefore not be used to accurately constrain the timing or magnitude of past landscape transience, but the ratio can be used to establish that transience did occur (Mudd, 2017). Depth profiles of CNs with similar proportions and types of production mechanisms do not add independent information on the exhumation history (Mudd, 2017), and thus cannot be used to extract specifics about past landscape transience (e.g. timing or magnitude of change in erosion rate). Depth profiles in sedimentary units emplaced at an independently known age can, however, be used to constrain the magnitude and/or timing of an erosional event (Fülöp et al., 2015). Generally, if the timing of a past event can be independently determined, the magnitude of the landscape transience can be robustly constrained, or vice versa.

In this paper, apparent erosion rates are defined to be significantly different when estimated apparent erosion rates do not overlap at the 1-σ level. Estimates of the CN concentration in a sample are subject to a number of uncertainties and possible error sources, including errors and uncertainties related to the sampling, lab preparation and AMS measurements. Additional uncertainties must be considered when translating a CN concentration into an apparent erosion rate, including those associated with estimating production rates. Translation of CN concentration into an apparent erosion rate moreover assumes that the CN concentration in a sample is solely a function of the production rate, erosion rate, and radioactive decay, and that other processes that may influence the CN concentration, e.g. burial, partial shielding by ice, vegetation etc., had negligible influence on the CN concentration. When estimating apparent erosion rate, the measured CN concentration must thus be assigned a total uncertainty to represent the unknown effect of all these factors. In this paper, we explore the condition under which landscape transience is detectable using paired measurements of in situ ^{14}C and ^{10}Be with total uncertainties of 2.5%, 5%, and 10%.

Eq. (4) indicates that estimates of apparent erosion rates are relatively precise when $\varepsilon\rho/\Lambda \gg \lambda\varepsilon$ (Fig. 2), i.e. in relatively rapidly eroding landscapes. If $\varepsilon\rho/\Lambda < \lambda$, such as for short-lived nuclides in relatively slowly eroding landscapes, the CN concentration is to a larger degree controlled by the rate of radioactive decay than by removal of nuclides through erosion, and even small uncertainties in the CN concentration result in large uncertainties in the estimated apparent erosion rate (Fig. 2). In situ ^{14}C is thus insensitive to erosion rates below 10 mm/kyr (Fig. 2), and only weakly sensitive to erosion rates below ~50–100 mm/kyr (Fig. 2) (von Blanckenburg, 2006). In contrast, estimates of erosion rates using longer-lived or stable nuclides are accurate even for very slow erosion rates (< 1 mm/kyr for ^{26}Al, < 0.5 mm/kyr for ^{10}Be and stable nuclides) (Fig. 2).

As the uncertainties in estimating apparent erosion rates depend on the CN concentration, the minimum/maximum $\varepsilon_C/\varepsilon_{Be}$ ratio, (i.e., the apparent erosion rate estimated using in situ ^{14}C divided by the apparent erosion rate estimated using ^{10}Be) required to detect a change varies with the CN concentration (Fig. 3). Specifically, in order to detect a change in erosion rate, the $\varepsilon_C/\varepsilon_{Be}$ ratio must deviate more from 1 in slowly eroding landscapes than in faster eroding landscapes. In rapidly eroding landscapes CN concentrations are however quite low. A larger sample mass must thus be measured on the AMS to separate the measured isotope ratio reliably from the blank. This problem can be avoided for ^{10}Be simply by dissolving more of the sample. For ^{14}C however, analysis is mass limited, typically to 5 g. As a result of this, ^{14}C uncertainties are somewhat higher in rapidly eroding landscapes. At the current analytical standard, analytical uncertainties exceed 10% and 20% for concentrations below $3{\cdot}10^4$ g and $1.5{\cdot}10^4$g respectively (Hippe, 2017), corresponding to SLHL steady-state erosion rates of 430 mm/kyr and 930 mm/kyr respectively.

2.3. Three models for the Late Pleistocene to Holocene erosion history

Using Eq. (1) and Eq. (4), the apparent erosion rate and

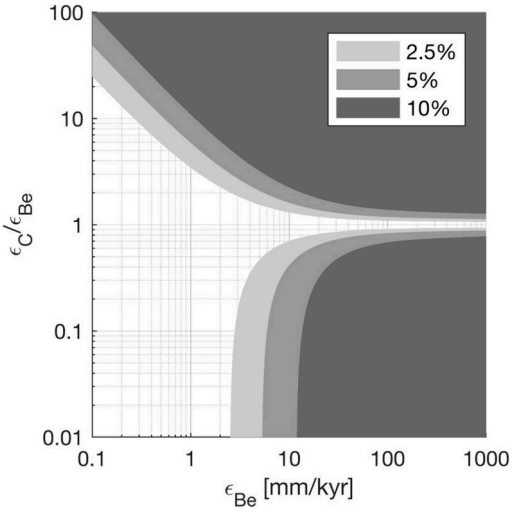

Fig. 3. The ability to detect change using paired measurements of in situ ^{10}Be and ^{14}C. Shaded areas enclose combinations of ε_{Be} and $\varepsilon_C/\varepsilon_{Be}$ where detection of a difference is possible, while detection of a difference is not possible in the unshaded areas. E.g., if ε_{Be} is estimated to be 1 mm/kyr, $\varepsilon_C/\varepsilon_{Be}$ must be at least 10 (i.e. ε_C is 10 mm/kyr) for the offset between ε_C and ε_{Be} to be significant given 5% uncertainty on the CN concentrations of both nuclides. Calculated for SLHL production rates.

corresponding uncertainty can be calculated for any erosion history and for any combination of cosmogenic nuclides. Furthermore, if the erosion history is represented by a set of model parameters, the parameter space for which landscape transience is detectable using the $\varepsilon_C/\varepsilon_{Be}$ ratio can be mapped. Here, we map the parameter space for three models for Late Pleistocene to Holocene erosion (Fig. 4) and show when landscape transience can be detected as a function of timing, magnitude, and style of erosion regime.

In the Step-Change (SC) model (Fig. 4a) a sudden change in erosion rate occurs at time t_{change}. The SC model thus simulate landscape transience as might have occurred due to, for example, increased fire frequency, increased soil-erosion due to the introduction of agriculture or other human activity, or initiation of a threshold process.

The Glacial-Interglacial (GI) model is designed to model how episodic changes between cold (glacial) and warm (interglacial) conditions during the Quaternary might have impacted erosion rates. To simulate this, the erosion rates in the GI model alternate between two piecewise constant erosion rates ε_{cold} and ε_{warm} (Fig. 4b), with the timing of the changes between cold and warm conditions being determined by past changes in global climate. Here, we use a smoothed version (a 5-kyr triangle filter) of the $\delta^{18}O$ benthic stack of Lisiecki and Raymo (2005) as a proxy for past changes in global climate (Fig. 4e). The smoothing acts as a low-pass filter, reducing the effects of short-term fluctuations that become negligible when the nuclide concentration is integrated over several thousand years. The parameter, t_{change}, which represents the timing of the last change in erosion rate, is used to divide the Quaternary into periods of ε_{cold} and ε_{warm}, as the $\delta^{18}O$ value at t_{change} is used as a threshold value between cold and warm periods. This implies that a landscape where t_{change} = 5 kyr experienced cold periods for a larger part of the Quaternary than a landscape where t_{change} = 15 kyr.

The gradual-change (GC) model is designed to explore how gradual, as opposed to abrupt, changes in erosion rate can be detected using the $\varepsilon_C/\varepsilon_{Be}$ ratio (Fig. 4c). The GC model simulates a gradual change in erosion rates, as might have occurred due to gradual changes in climatic conditions, or due to gradual response of the governing erosion processes to changes in climate. In the GC model, the erosion rate is a linear function of a normalized $\delta^{18}O$ value:

$$\varepsilon(t) = k_{mean}(k_{var}(\delta^{18}O_{norm}(t)) + 1) \quad (5)$$

Here, k_{mean} is the average erosion rate over several glacial-interglacial cycles, k_{var} indicates the correlation between climate and erosion rates [-1 < k_{var} < 1], and $\delta^{18}O_{norm}(t)$ is a normalized version of the 5 kyr triangle-smoothed $\delta^{18}O$ record, defined as

$$\delta^{18}O_{norm}(t) = \frac{\delta^{18}O(t) - (\delta^{18}O_{max} + \delta^{18}O_{min})/2}{(\delta^{18}O_{max} - \delta^{18}O_{min})/2} \quad (6)$$

$\delta^{18}O_{norm}(t)$ thus varies between −1 and 1 (Fig. 4e). Negative values of k_{var} indicate that erosion is faster during warm periods (negative $\delta^{18}O_{norm}$ values) than during cold periods (positive $\delta^{18}O_{norm}$ values), while a positive k_{var} means that erosion is fastest during cold periods.

3. Results

We begin by studying the temporal response to a sudden increase or decrease in erosion rate using the SC model (Fig. 5). Subsequently, we map detectable erosion histories on Late Pleistocene to Holocene timescales using the three erosion models (Figs. 6–8). The results presented are calculated using SLHL production rates (Table 1). At higher

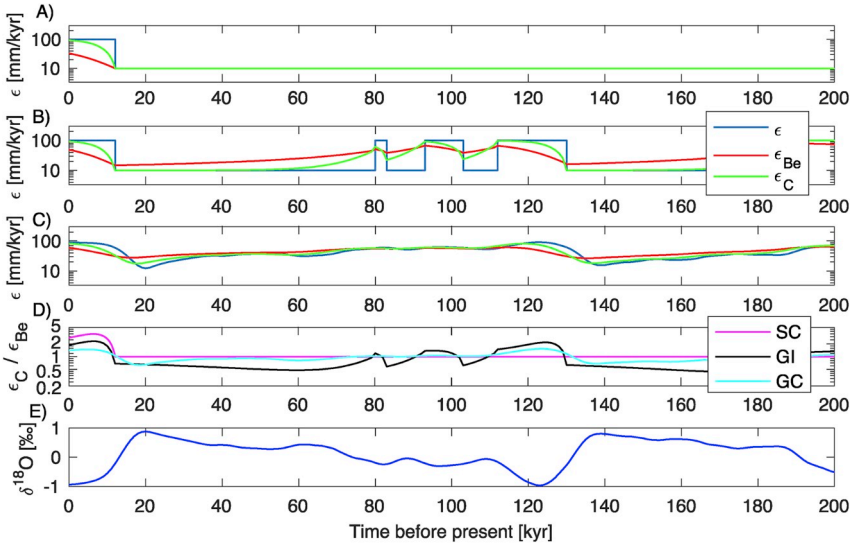

Fig. 4. Forward models and apparent erosion rates. a) Step Change (SC) model, b) Glacial Interglacial (GI) model c) Gradual Change (GC) model. Blue lines are the actual erosion rates, red lines are ε_{Be}, green lines are ε_C. d) $\varepsilon_C/\varepsilon_{Be}$ ratio, e) normalized, 5kyr smoothed $\delta^{18}O$ benthic stack (Lisiecki and Raymo, 2005).

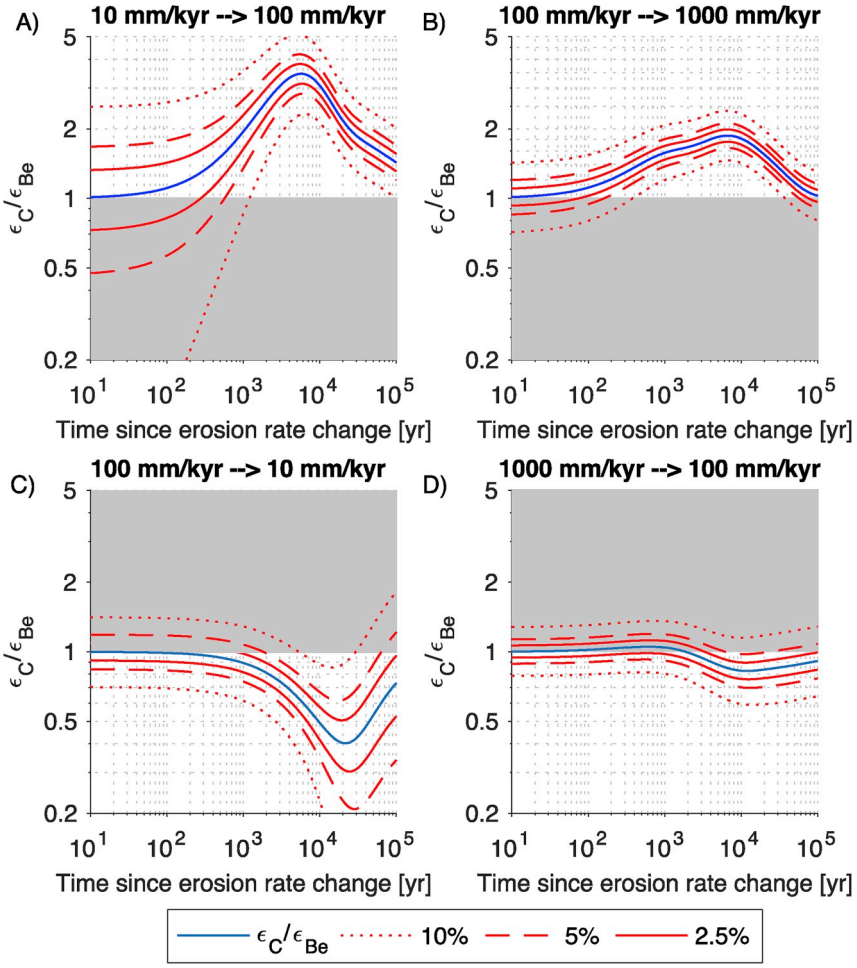

Fig. 5. Evolution of $\varepsilon_C/\varepsilon_{Be}$ following tenfold changes in erosion rate. Blue line is $\varepsilon_C/\varepsilon_{Be}$, while the solid, dashed and the dotted red lines represent 2.5, 5% and 10% uncertainty respectively. When both the upper and lower limit at a given uncertainty is outside the shaded area, the change in erosion rate is detectable at the uncertainty level, e.g. an increase in erosion rate from 10mm/kyr- > 100 mm/kyr (subplot A) can be detected from 1.2kyr until 100kyr after the increase for 10% uncertainty. This figure is similar to Fig. 2 from Mudd (2017), but includes uncertainties on CN concentrations and the effect of muons. Calculated using SLHL production rates.

elevations, spallogenic production accounts for a relatively higher fraction of the total production, and the effects of muogenic production thus become less important at higher altitudes (Appendix A). All erosion rates are calculated for surface materials with a density of 2.6 g cm^{-3}. In landscapes with surface materials of different densities, the erosion rates reported here must be scaled. For instance, an erosion rate of 10 mm/kyr in this study corresponds to an erosion rate of 16.25 mm/kyr in a soil-mantled landscape with a soil density of 1.6 g cm^{-3}.

3.1. $\varepsilon_C/\varepsilon_{Be}$ following a step-change in erosion rate

A past step-change in erosion rate can be detected using the $\varepsilon_C/\varepsilon_{Be}$ ratio provided one of the CNs retain a stronger "memory" of the past erosion rate than the other CN, and that estimates of erosion rate using both CNs are accurate enough. The "memory" of a CN depends on both the half-life of the nuclide and the erosion rate, but also on the relative importance of different production mechanisms. In most landscapes, a change in erosion rate would result in ε_C quickly tending towards the new actual erosion rate, before reaching near secular equilibrium in under 25 kyr, while ε_{Be} needs more time to equilibrate (Fig. 5). In other words, the ratio of apparent erosion rates, $\varepsilon_C/\varepsilon_{Be}$, evolves in time after a change in actual erosion rates, until the concentration of ^{10}Be has also equilibrated to the new erosion rate. The possibility of detecting a change in erosion rate thus depends on the magnitude and the timing of the change. For the ^{14}C-^{10}Be pair, the window for detecting a step-change in erosion rate at a statistically significant level spans the Late Pleistocene and Holocene for typical erosion rates (Fig. 5), and the $\varepsilon_C/\varepsilon_{Be}$ ratio is thus useful for studying changes in erosion rate during this time period. For example, given 10% uncertainty on the CN concentrations, a tenfold increase in erosion rate from 10 mm/kyr to 100 mm/kyr, as might occur due to deforestation and introduction of agriculture (Montgomery, 2007), is detectable from 1.2 kyr after the change until 100 kyr after the change, while a tenfold decrease in erosion rate, as might occur when a landscape is no longer under tillage (Montgomery, 2007), from 100 mm/kyr to 10 mm/kyr is detectable from 6 kyr after the change until 28 kyr after the change (Fig. 5). For lower uncertainties on the CN concentrations, the detection window is longer.

Muogenic production only accounts for a small fraction of the total surface production rate (SLHL: ~2%) of ^{10}Be and ^{26}Al (Balco, 2017; Borchers et al., 2016; Braucher et al., 2011, 2003), while it accounts for ~23% of the surface production rate of in situ ^{14}C (Balco, 2017; Heisinger et al., 2002b, 2002a; Lupker et al., 2015). The muogenic production of CNs is important in some specific cases, as it can influence the length and timing of the window where detection is possible. This is especially true for settings close to sea level, where the muogenic production contributes more to the total production compared to higher elevations (Appendix A). Furthermore, muogenic production is also important in landscapes that are currently rapidly eroding, but used to

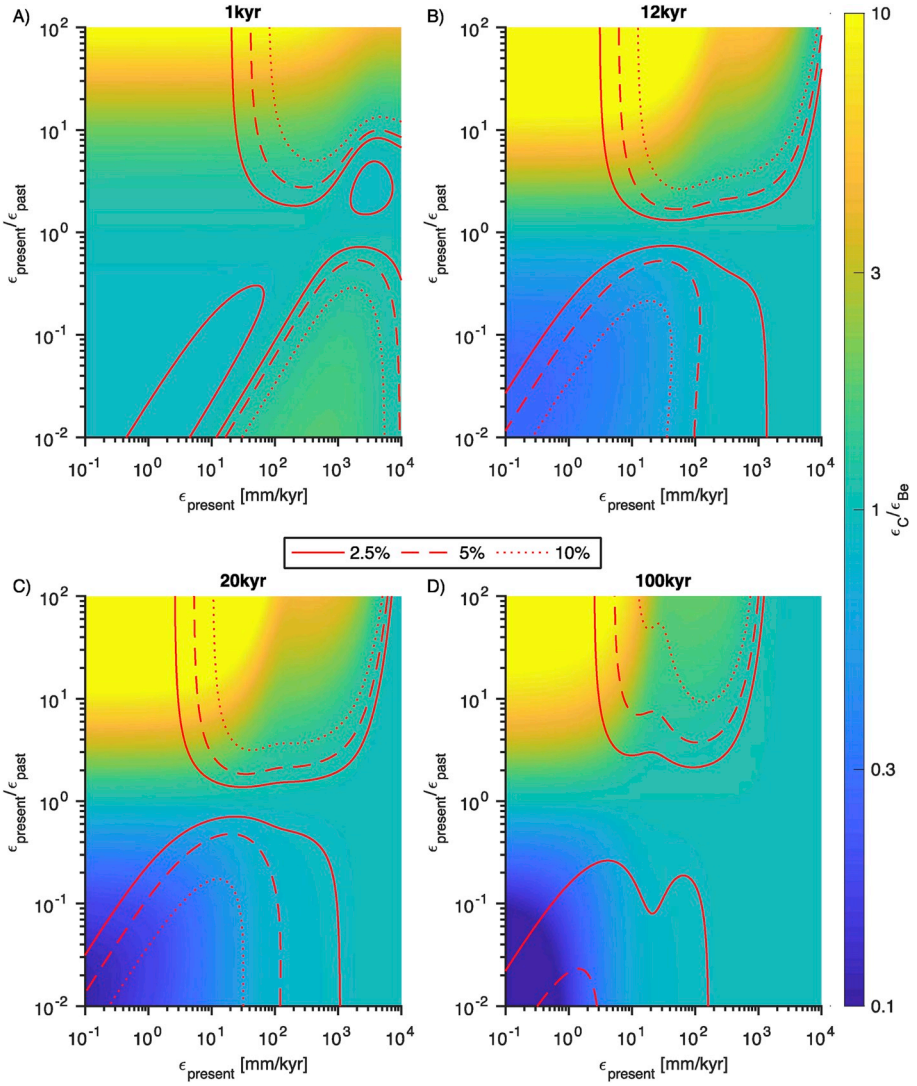

Fig. 6. Mapping of the $\varepsilon_C/\varepsilon_{Be}$ ratio for the SC model. Red lines surround parameter combinations where the change in erosion rate is detectable at the given uncertainty estimation (smaller uncertainties correspond to a larger enclosed areas). Note from A) that ε_C initially adjusts more slowly than ε_{Be} to changes in erosion rate in rapidly eroding landscapes. This is especially true for past decreases in erosion rate. Calculated using SLHL production rates.

erode at a slower rate. This is due to two factors: 1) In rapidly eroding landscapes, samples spend only short time near the surface where spallogenic production dominates, causing CN inventories to be more influenced by muogenic production relative to samples from slowly eroding landscapes, and 2) samples that experienced a past increase in erosion rate spent relatively more time at depth (when erosion rates were slow) than in the upper surface (when erosion rates were faster), resulting in an increased proportion of muogenic CNs in the surface inventory. A consequence of this effect is that inclusion of muogenic production extends the period where an increase in erosion rate from 100 mm/kyr to 1000 mm/kyr is detectable from 0.4 to 1.5 kyr (Appendix A) to 0.4–38 kyr (Fig. 5b). The production of CNs by muons is less important in landscapes that experienced a decrease in erosion rate. For example, a decrease in erosion rate from 100 mm/kyr to 10 mm/kyr can be detected from 5 kyr after the change until 28 kyr after the change in the absence of production due to muons (Appendix A), which is similar to what is found when including muogenic production (from 6 kyr until 28 kyr after the change) (Fig. 5c).

3.2. Detecting changes in erosion rate on Late Pleistocene to Holocene timescales

Given that the $\varepsilon_C/\varepsilon_{Be}$ ratio is suitable for detecting changes in erosion rate on Late Pleistocene to Holocene timescales, we map the parameter combinations for which landscape transience is detectable by calculating the $\varepsilon_C/\varepsilon_{Be}$ ratio for a large range of model parameters. We do so for all three models of erosional transience described above. The mapping of the different models, with multiple choices of t_{change}, show to what degree landscape transience with different timings, magnitudes, and styles of transience (Figs. 6–8) is detectable.

Generally, all three mappings (Figs. 6–8) show that 1) the $\varepsilon_C/\varepsilon_{Be}$ can be used to detect landscape transience for a wide range of exhumation histories, 2) the $\varepsilon_C/\varepsilon_{Be}$ ratio deviates more from unity for larger changes in erosion rate, implying that the possibility of detecting a change is better for larger changes in erosion rate, 3) for higher uncertainties in nuclide measurements, the range of detectable changes in erosion rate is narrower, and 4) landscape transience on Late Pleistocene to Holocene timescales cannot be detected in very slowly or very rapidly eroding landscapes using the $\varepsilon_C/\varepsilon_{Be}$ ratio.

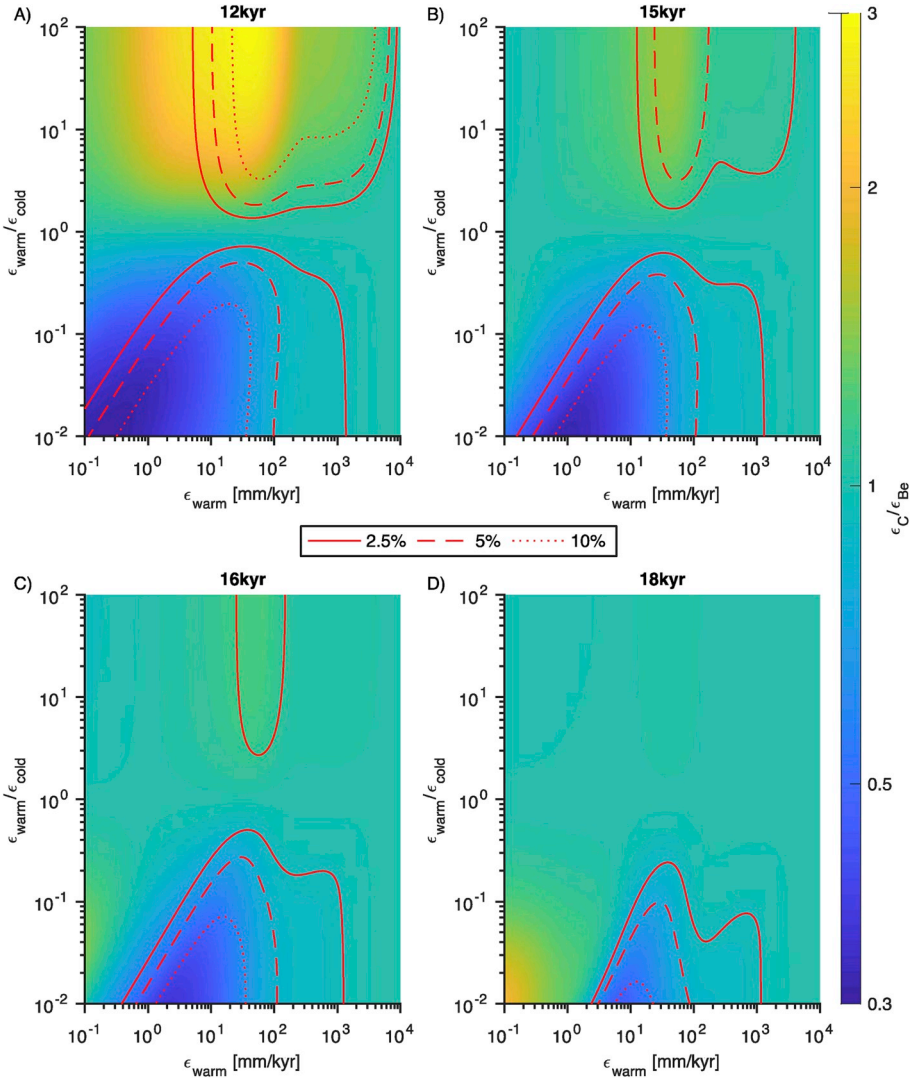

Fig. 7. Mapping of the $\varepsilon_C/\varepsilon_{Be}$ ratio for the GI model. Red lines surround parameter combinations where the change in erosion rate is detectable at the given uncertainty estimation (smaller uncertainties correspond to a larger enclosed areas). t_{change} corresponds to durations of the last period of ε_{Cold} of 68kyr for t_{change} = 12kyr, 27kyr for t_{change} = 15kyr, 14kyr for t_{change} = 16kyr and 4kyr for t_{change} = 18kyr. Calculated using SLHL production rates.

3.2.1. The step-change model

The individual mappings give nuance to these general results, and reveal the effect of timing and style of transience. The mapping of the SC model (Fig. 6) shows that a step-change in erosion rate occurring within the last 100 kyr is detectable in landscapes eroding at a wide range of erosion rates. For example, an increase in erosion rate by more than a factor of 2 during the last 12–20 kyr is detectable in landscapes that currently erode at rates between 5 and 2000 mm/kyr, given an uncertainty of 2.5% on the CN concentrations and assuming SLHL production rates (Fig. 6). However, as described above, the analytical uncertainty of ^{14}C is a function of the ^{14}C concentration due to sample size limitations. As a result, erosion rates estimates using ^{14}C are more uncertain in rapidly eroding landscapes. Given current analytical standards, the detection window of a doubling of the erosion rate during the last 12–20 kyr narrows to landscapes currently eroding between 5 and 500 mm/kyr, as the analytical uncertainties in samples from landscapes eroding at 500 mm/kyr would exceed 10%, limiting the ability to detect a change. The mapping of the SC model thus demonstrates how uncertainty in estimating apparent erosion rates using CN concentrations impacts the ability to detect landscape transience. Naturally, smaller uncertainties enable detection of landscape transience at a wider range of timings, magnitudes, and erosion rates. This highlights that assigning a realistic estimate of the total nuclide uncertainty is critical for detecting landscape transience, as underestimations of uncertainty can result in false positive detections, while overestimations of uncertainty can prevent detection. It is thus important to account for uncertainties relating to sampling, laboratory work, AMS measurements, as well as uncertainties in the production rates via different production mechanisms. Furthermore, it is important to identify, and if possible correct for, other processes that may influence nuclide concentrations, such as partial or complete burial by ice, snow, dunes, soil, or vegetation, or effects of chemical weathering (Riebe and Granger, 2013).

3.2.1.1. Detecting landscape transience in slowly eroding landscapes. The SC mapping also highlights that detection of landscape transience is inherently difficult in slowly eroding landscapes (< 5–20 mm/kyr, depending on uncertainties) because the in situ ^{14}C concentration may reach secular equilibrium (Fig. 2). As a result, past landscape transience is not detectable in landscapes that are currently eroding more slowly than ~5 mm/kyr, regardless of how low the uncertainties on the CN concentrations are. An exception is the detection of past decreases in erosion rates, which can be detected as long as the ^{10}Be concentration "remembers" the faster erosion rate from before the

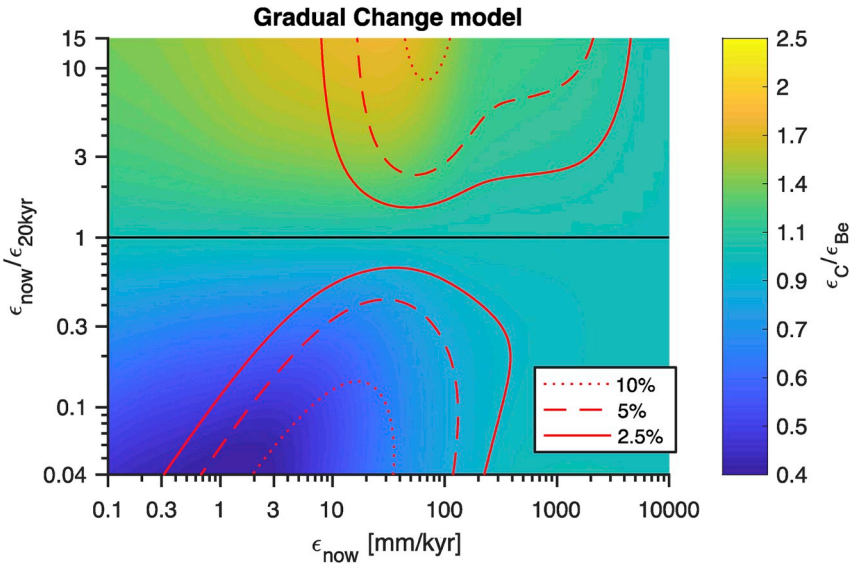

Fig. 8. Mapping of the $\varepsilon_C/\varepsilon_{Be}$ ratio for the Gradual Change model. The x-axis is the current erosion rate ε(0kyr). The y-axis is the current erosion rate divided by the erosion rate 20kyr ago (ε(0kyr)/ε(20kyr)). Red lines surround parameter combinations where the change in erosion rate is detected at the given uncertainty estimation (smaller uncertainties correspond to a larger surrounded areas). Calculated using SLHL production rates.

change.

3.2.1.2. Detecting landscape transience in rapidly eroding landscapes. The ability to detect landscape transience on Late Pleistocene to Holocene timescales using the $\varepsilon_C/\varepsilon_{Be}$ ratio is also difficult in rapidly eroding landscapes because the "memory" of past changes becomes short, i.e. ^{10}Be also adjusts quickly to near-secular equilibrium in rapidly eroding landscapes. CNs produced prior to a change are quickly removed by erosion, and landscape transience might thus only be detectable for a few kyr in landscapes eroding more rapidly than ~500 mm/kyr. Interestingly, the in situ ^{14}C concentration is initially slower to adjust to changes in erosion rate than the ^{10}Be concentration in rapidly eroding landscapes (Fig. 6a). This is due to differences in the relative importance of production by spallation and by muogenic pathways for in situ ^{10}Be and ^{14}C. For changes in erosion rate in rapidly eroding landscapes, this comparatively larger muogenic memory of deep production for in situ ^{14}C than for ^{10}Be dominates the effect associated with different rates of radioactive decay in the first few kyr after a change in erosion rate, especially in landscapes that experienced a past decrease in erosion rate. As a result, ^{10}Be initially adjusts more quickly to landscape transience than in situ ^{14}C in such landscapes, which can result in false interpretations of the direction of past changes in erosion rate in rapidly eroding landscapes.

3.2.2. The glacial-Interglacial model

The GI model simulates the effect of past variations in erosion rate over multiple glacial-interglacial cycles, and shows when these variations can be detected using the $\varepsilon_C/\varepsilon_{Be}$ ratio. The mapping of the GI model (Fig. 7) shows the same general pattern as the SC model. A main difference between the SC and the GI models is that, for the same fractional change in erosion rate, the $\varepsilon_C/\varepsilon_{Be}$ ratio deviates less from 1 in the GI than in the SC model. For instance, a change in erosion rate from 10 mm/kyr to 100 mm/kyr that occurred 12 kyr ago results in a $\varepsilon_C/\varepsilon_{Be}$ ratio of 2.85 in the SC model (Fig. 6), but only a $\varepsilon_C/\varepsilon_{Be}$ ratio of 1.85 in the GI model (Fig. 7). This difference in $\varepsilon_C/\varepsilon_{Be}$ between the models is due to inheritance of ^{10}Be nuclides from prior periods with alternating erosion rates, i.e. past periods with erosion rates of 100 mm/kyr and 10 mm/kyr in example above. Due to this memory of past periods characterized by alternating erosion rates, the range of parameter combinations for which landscape transience is detectable using the $\varepsilon_C/\varepsilon_{Be}$ ratio is narrower for the GI model than for the SC model.

The other main difference between the SC and the GI model is that the effect of t_{change} differs between the models. While t_{change} just represents the timing of a single step-change in erosion rate in the SC model, t_{change} controls a long series of past transitions in erosion rate in the GI model. If t_{change} is 12 kyr in the GI model, the last period of cold-weather erosion was 68 kyr long (Fig. 7a), but only 4 kyr long if t_{change} is 18 kyr (Fig. 7d). Fig. 7 shows that landscape transience is detectable for a much larger range of ε_{cold} and ε_{warm} for t_{change} = 12 kyr than for t_{change} = 18 kyr. This goes to show that the long-term erosional history of the landscape is important for the ability to detect past landscape transience, and that short-term perturbations of the erosion rate around the time of LGM are not easily detected today using measurements of the $\varepsilon_C/\varepsilon_{Be}$ ratio in surface samples.

3.2.3. The gradual-change model

Like the SC and GI models showed that abrupt changes in erosion rate are detectable for many erosional histories, the mapping of the GC model shows that a gradual change in erosion rate from the time of the LGM until now is also detectable using the $\varepsilon_C/\varepsilon_{Be}$ ratio (Fig. 8). As for the GI model, the $\varepsilon_C/\varepsilon_{Be}$ ratio of the GC model deviates less from 1 for a given fractional change in erosion rate than for the SC model, but still differs enough from 1 to be detectable for many parameter combinations.

4. Discussion

Our results confirm that landscape transience on Late Pleistocene to Holocene timescales can in many cases be detected by paired measurements of a short-lived CN like in situ ^{14}C and a long-lived or stable CN, such as ^{10}Be, ^{26}Al, or ^{21}Ne. The results expand upon earlier studies of Mudd (2017) and Hippe (2017) in a number of ways, in that:

1) We include uncertainties on the nuclide concentrations to study their influence on the ability to detect landscape transience (Fig. 2).
2) We include the muogenic production of CNs, which has implications, both for the length of the timeframe where detection of landscape transience is possible (Fig. 5, Appendix A) and for the possibility of detecting changes in rapidly eroding landscapes (Fig. 6a).
3) We study how different styles of Quaternary erosion (Fig. 5) affect the possibility of detecting landscape transience using in situ ^{14}C

and ^{10}Be (Figs. 6–8).

The inclusion of these additional factors adds new insights to the analyses presented in Mudd (2017) and Hippe (2017). For example, the inclusion of non-linear uncertainties in estimating apparent erosion rates reveals that the $\varepsilon_C/\varepsilon_{Be}$ ratio is not suitable for detecting landscape transience in slowly eroding landscapes (Fig. 3). Furthermore, the inclusion of muogenic production extends the time window in which landscape transience is detectable (Fig. 5, Appendix A). Furthermore, the relatively larger fraction of production by muons for in situ ^{14}C than ^{10}Be can result in false interpretations of the direction of past landscape transience in rapidly eroding landscapes if the muogenic production is not accounted for (Fig. 6a).

These results are based on the SLHL muogenic production rates for ^{10}Be and ^{26}Al from Balco (2017) and in situ ^{14}C from Heisinger et al. (2002b, 2002a), which are consistent with estimates from Balco (2017) and Lupker et al. (2015). At higher elevations, the contribution of muons to the total production is smaller than at sea level, implying that the effects of muogenic production discussed above decrease with increasing altitude (Appendix A). Similarly, some field data suggest that the fraction of SLHL production by muons might be smaller than the values used in this paper (Braucher et al., 2013). This would similarly decrease the effect of muogenic production discussed above. The three test scenarios for Quaternary changes in erosion (Figs. 6–8) show that the $\varepsilon_C/\varepsilon_{Be}$ ratio can be used to detect landscape transience for a wide range of uncertainties and for many different timings and styles of landscape transience.

4.1. Applicability to natural landscapes

The $\varepsilon_C/\varepsilon_{Be}$ ratio is suitable for detecting both abrupt, gradual, and/or repeated changes in erosion rate, and is thus versatile and robust enough for studies of many types of landscape histories on Late Pleistocene to Holocene timescales. The results are valid in continuously exposed landscapes, but are not applicable to landscapes that have for example experienced periods of burial or soil mixing unless a suitable correction of the CN concentrations can be made.

In mid- and low-latitude regions that were not directly affected by continental ice sheets, the time-window where detection of landscape transience using the paired chronometers is possible corresponds to the timing of major shifts in vegetation dynamics and temperature that are known to have strongly influenced erosion (e.g. Marshall et al., 2015). Moreover, the human transformation of the environment through use of fire and spread of agriculture led to unprecedented changes in erosional dynamics (e.g. Syvitski, 2003). Milliman and Syvitski (1992) estimate that human impacts due to deforestation and farming have doubled the sediment production in small upland catchments farmed since 2500-2000 yr BP. As opposed to studies of such processes using sedimentary archives, where source-to-sink coupling might obscure e.g. environmental signals (Jerolmack and Paola, 2010), the ^{14}C-^{10}Be method can be used to study such dynamics in situ where the change in erosion rate occurred, and provide point measurements of erosional transience. Several samples from across a landscape thus need to be analysed to study landscape-wide transients. However, the method can be used to detect regional changes of denudation rates in suitable catchments, allowing for broader interpretations about regional landscape evolution (von Blanckenburg, 2006). If in situ ^{14}C is used to estimate catchment-wide denudation rates, we recommend that the measurements of in situ ^{14}C in stream samples are combined with measurements from the surrounding hillslopes and stream terraces to help disentangle whether a disequilibrium between in situ ^{14}C and ^{10}Be concentrations is due to changes in erosion rate, soil mixing, periods of burial/transport, or other factors. Estimates of catchment-averaged erosion rates can furthermore be combined with lake core samples of in situ ^{14}C and ^{10}Be to obtain denudation rates back in time. This would enable even more detailed studies that perhaps can constrain both the timing and the magnitude of past changes in erosion rate.

4.2. Choice of CNs

While the results in this study are based on the combination of in situ ^{14}C (due to its short half life) and ^{10}Be (due to its long half-life and routine measurement), ^{26}Al or ^{21}Ne could replace ^{10}Be with largely similar results (Appendix B). However, combinations of nuclides excluding ^{14}C (or another similarly short-lived nuclide) are not suitable for detecting landscape transience on Late Pleistocene to Holocene timescales (Appendix B). The measurement of in situ ^{14}C is therefore critical for resolving landscape transience on Late Pleistocene to Holocene timescales. However, measurement of in situ ^{14}C remains technically challenging and few laboratories offer this possibility, although the number is increasing (Hippe, 2017). It may therefore be sensible to ensure that the ^{10}Be apparent erosion rate fits within the detection window before investing resources in measuring ^{14}C.

5. Conclusions

In this paper, we investigate the possibility for using in situ CN concentrations in rocks or sediment to detect changing erosion rates in continuously exposed fluvial landscapes on Late Pleistocene to Holocene timescales. We find that the ability to resolve past changes in erosion rate depends on a number of factors, including the timing, magnitude, and nature (abrupt vs. gradual) of the change. Our analysis highlights that CN concentrations are integral functions of the erosion rate history, as well as the production and decay rates of the nuclide, and that erosional transience can be detected from CN concentrations in hillslope and stream-sediment samples. However, prerequisites for detecting transience in landscape-wide denudation rates via stream-sediment samples include minimal soil mixing, negligible sediment storage relative to radioactive decay, and limited mass movement in the catchment (von Blanckenburg, 2006).

In general, our results show that:

1) Using combined measurements of ^{10}Be and in situ ^{14}C with standard uncertainties (2.5–10%), it is possible to detect large changes in erosion rates (factor > 2) in landscapes eroding at typical rates (5 mm/kyr – 500 mm/kyr).
2) The production of cosmogenic nuclides by muons is important for the ability to detect changes in erosion rate, particularly in rapidly eroding landscapes. Muogenic production should thus be considered when detecting erosional transience using paired nuclides.
3) Uncertainty in erosion rate estimates limits the ability to estimate erosion rates using ^{14}C in both slowly (due to saturation of the ^{14}C concentration) and rapidly eroding landscapes (due to blank subtraction and sample size limitations). Lowering the uncertainty in CN concentrations from 10% to 5% or less greatly improves the ability to resolve past changes in erosion rate.
4) Paired measurements of short-lived in situ ^{14}C with a longer-lived nuclide (^{10}Be, ^{26}Al or ^{21}Ne) can help to identify how climatic changes and human activity influenced erosion rates on Late Pleistocene to Holocene timescales.

6. Computer code

All calculations in this paper were done using MATLAB (R2017b).

MATLAB code to perform all calculations and generate all figures is available at the following address:

https://github.com/danielskov/14C_10Be_landscape_transience.

Conflicts of interest

The authors declare no conflicts of interest.

Acknowledgements

This study was supported by Independent Research Fund Denmark (grant number DFF-6108-00226). Andrew Hein, Jason P. Briner, Maarten Lupker and an anonymous reviewer are thanked for constructive comments and ideas that greatly improved the manuscript.

Appendix A

The importance of muogenic production. The time window where detection of landscape transience is possible becomes significantly shorter if muogenic CN production is ignored (Fig. A1). The fraction of muogenic production to the total production decreases with increasing altitude. At higher altitudes, the influence of muogenic production thus diminishes with increasing altitude (Fig. A2).

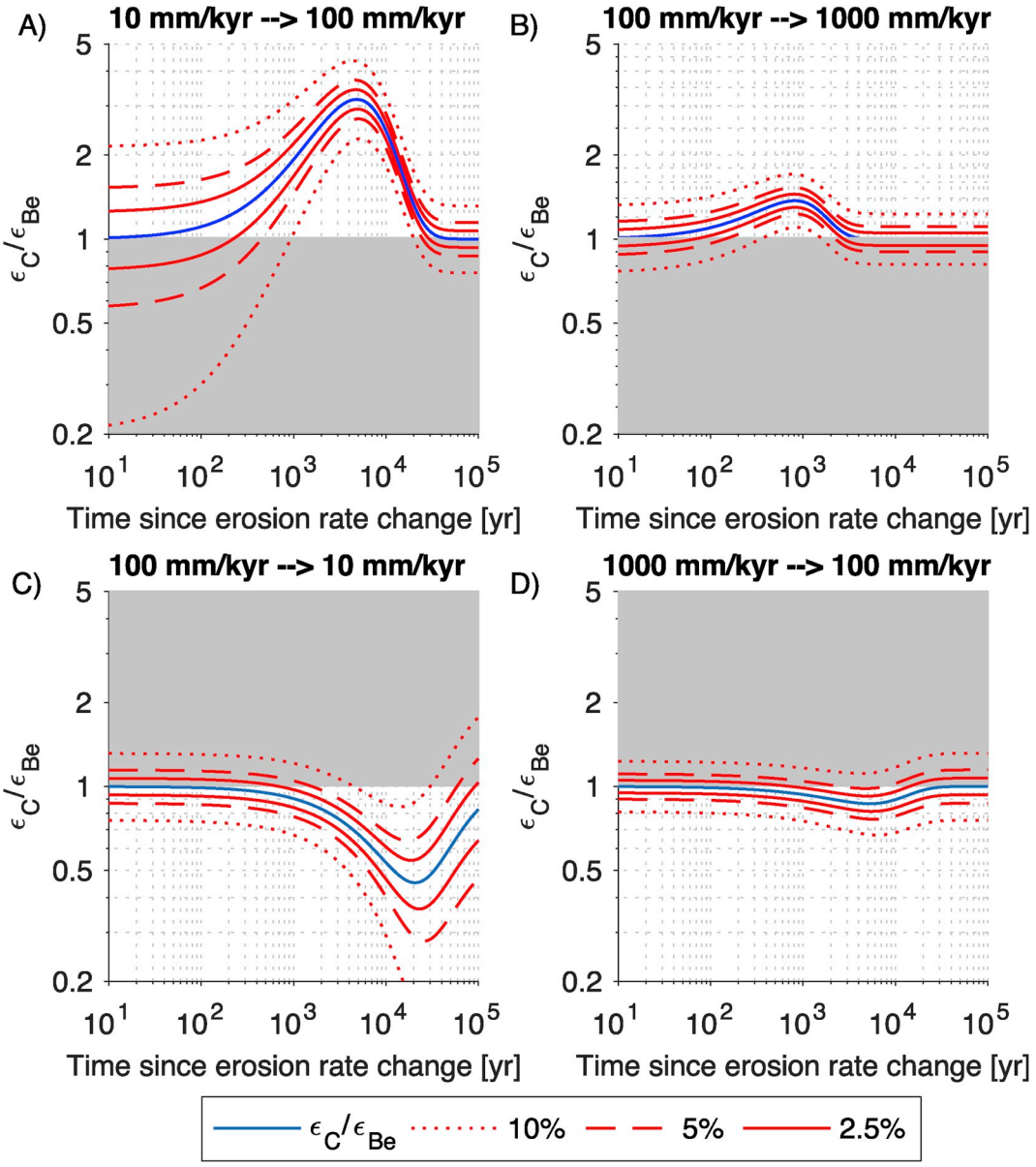

Fig. A.1. Adaption times given no muogenic production. The window where detection of landscape transience is possible is shifted and shortened compared to the case when production by muons is included (Fig. 5), especially in settings that experienced increases in erosion rate in the past.

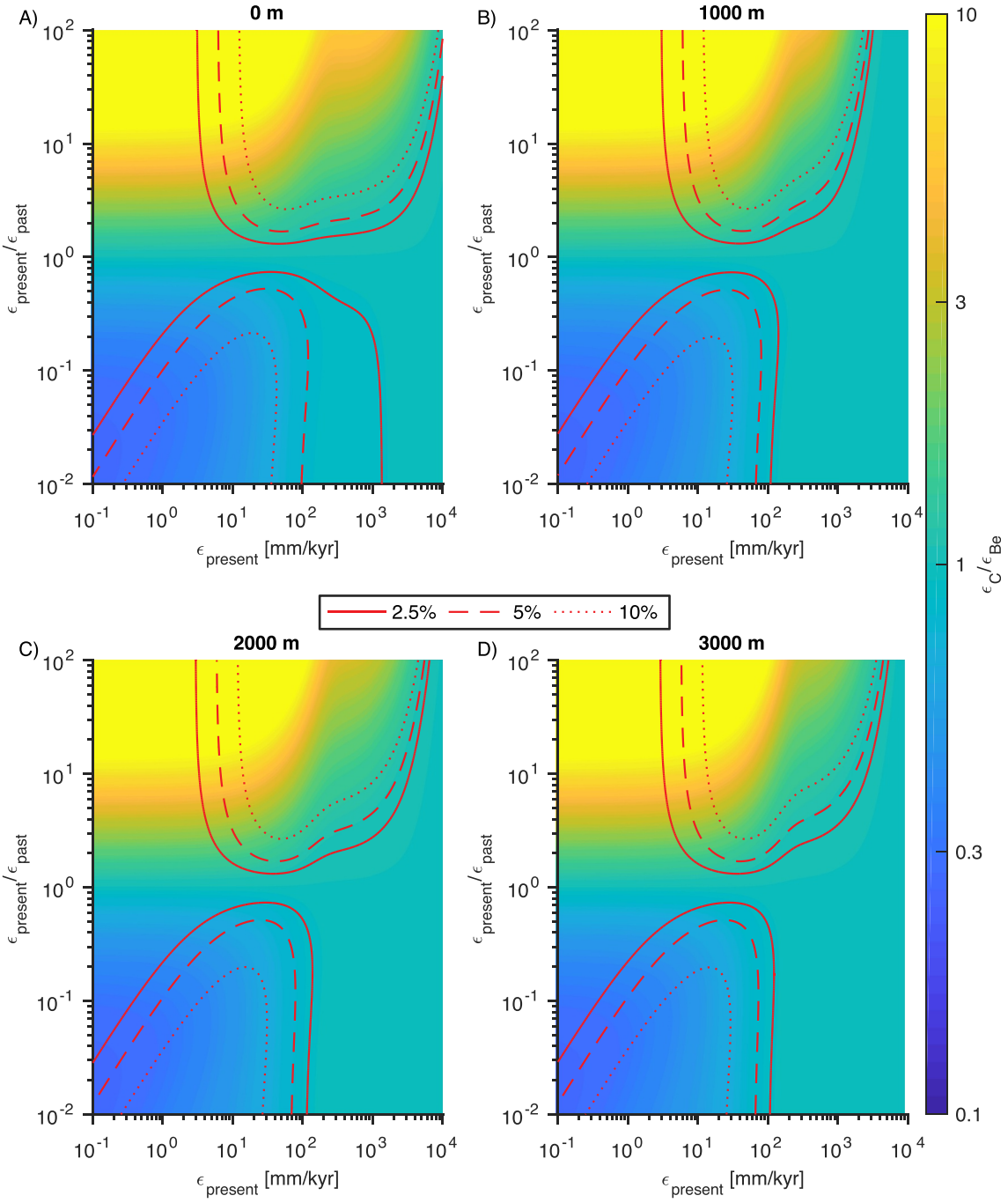

Fig. A.2. The effect of increasing altitude (elevations superscripts on each plot), and thus changes in production rates, in the SC model with t_{change} = 12kyr. At increasing elevations the muogenic production is of less and less importance, which lowers the upper limit of erosion rates in which landscape transience can be detected.

Appendix B

The choice of long-lived nuclide to be paired with in situ ^{14}C is not of great importance, and ^{10}Be can be substituted for another long-lived or stable nuclide (Fig. B1). However, in situ ^{14}C, or another similarly short-lived CN is essential for detecting landscape transience on Late Pleistocene to Holocene timescales, and cannot be substituted by a long-lived nuclide (e.g. ^{26}Al, Fig. B2).

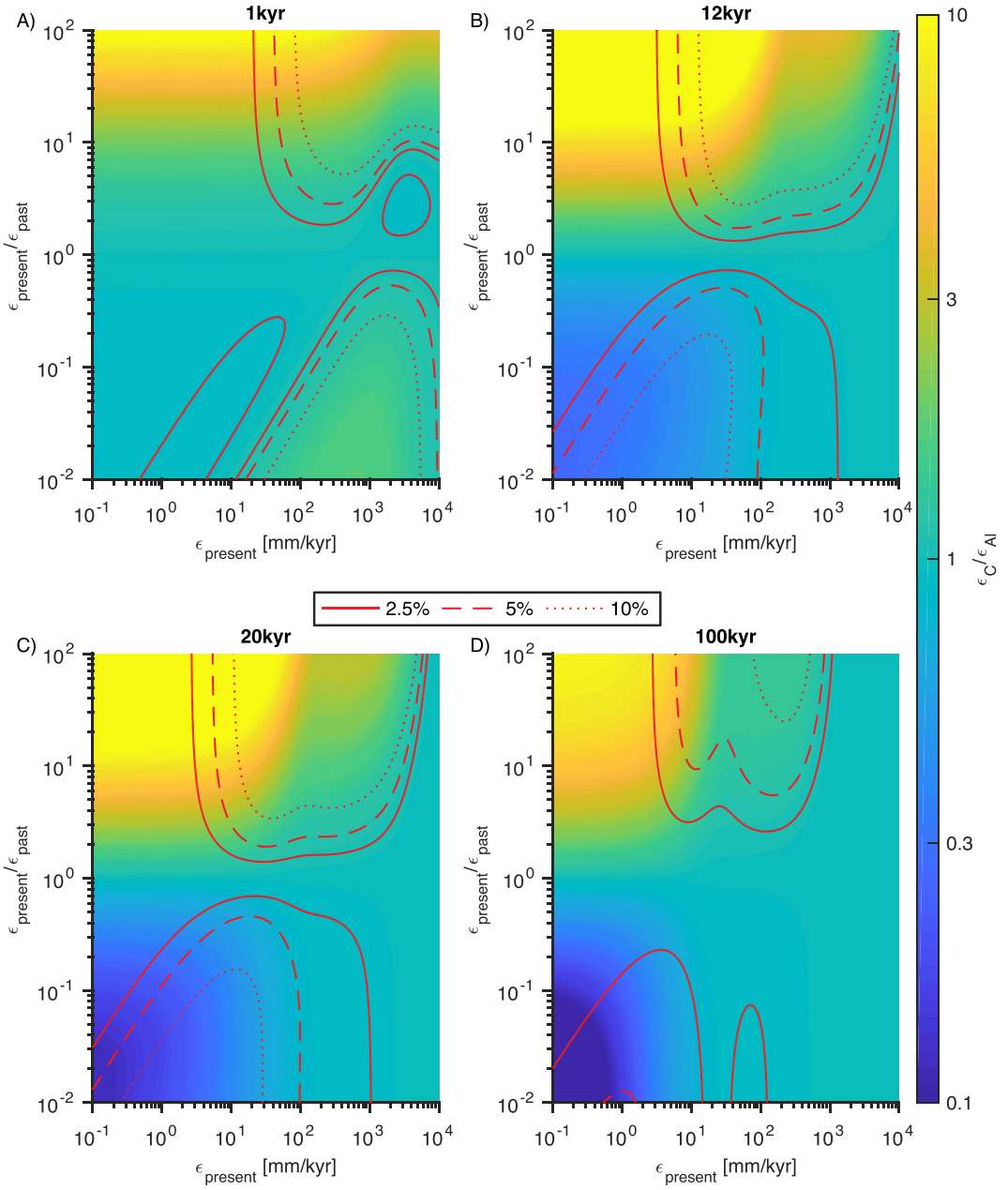

Fig. B.1. SC model with ^{26}Al and in situ ^{14}C. The pattern is very much the same as in Fig. 6, showing that the choice of long-lived nuclide (^{10}Be, ^{26}Al or ^{21}Ne) to be paired with in situ ^{14}C when trying to detect landscape transience is not important.

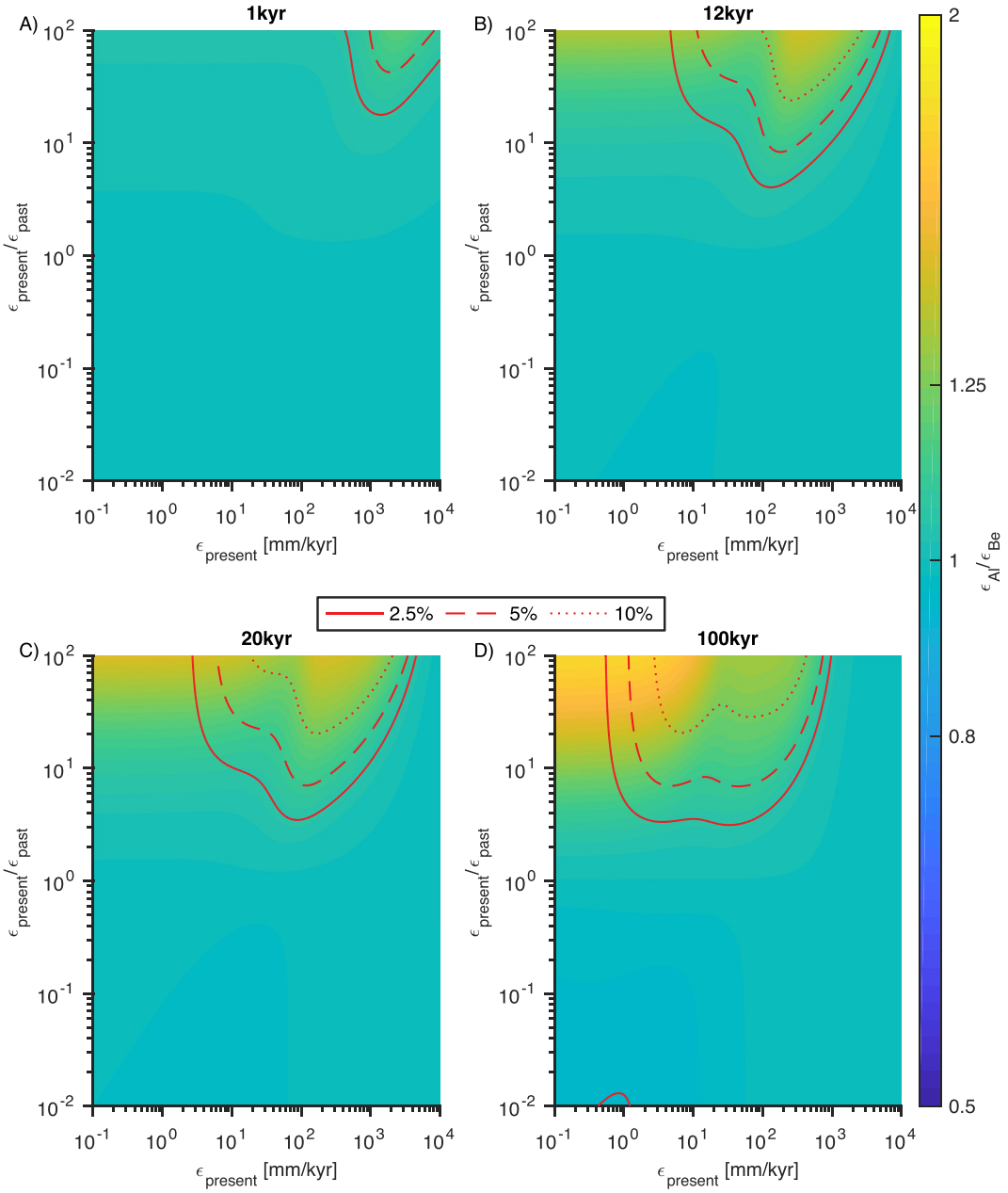

Fig. B.2. SC model with ^{26}Al and ^{10}Be. A change in erosion rate needs to be much bigger, and have happened much longer ago to be detected using this pair of nuclides, compared to the ^{10}Be and ^{14}C pair (Fig. 6).

References

Andersen, J.L., Egholm, D.L., Knudsen, M.F., Jansen, J.D., Nielsen, S.B., 2015. The periglacial engine of mountain erosion - Part 1: rates of frost cracking and frost creep. Earth Surf. Dyn. 3, 447–462. https://doi.org/10.5194/esurf-3-447-2015.

Balco, G., 2017. Production rate calculations for cosmic-ray-muon-produced10Be and26Al benchmarked against geological calibration data. Quat. Geochronol. 39, 150–173. https://doi.org/10.1016/j.quageo.2017.02.001.

Balco, G., Stone, J.O., Lifton, N.A., Dunai, T.J., 2008. A complete and easily accessible means of calculating surface exposure ages or erosion rates from 10Be and 26Al measurements. Quat. Geochronol. 3, 174–195. https://doi.org/10.1016/j.quageo.2007.12.001.

Bierman, P.R., Steig, E.J., 1996. Estimating rates of denudation using cosmogenic isotope abundances in sediment. Earth Surf. Process. Landf. https://doi.org/10.1002/(SICI)1096-9837(199602)21:2<125::AID-ESP511>3.0.CO;2-8.

Borchers, B., Marrero, S., Balco, G., Caffee, M., Goehring, B., Lifton, N., Nishiizumi, K., Phillips, F., Schaefer, J., Stone, J., 2016. Geological calibration of spallation production rates in the cronus-earth project. Quat. Geochronol. 31, 188–198. https://doi.org/10.1016/j.quageo.2015.01.009.

Braucher, R., Bourlès, D., Merchel, S., Vidal Romani, J., Fernadez-Mosquera, D., Marti, K., Léanni, L., Chauvet, F., Arnold, M., Aumaître, G., Keddadouche, K., 2013. Determination of muon attenuation lengths in depth profiles from in situ produced cosmogenic nuclides. Nucl. Instrum. Methods Phys. Res. Sect. B Beam Interact. Mater. Atomos. 294, 484–490. https://doi.org/10.1016/j.nimb.2012.05.023.

Braucher, R., Brown, E.T., Bourlès, D.L., Colin, F., 2003. In situ produced10Be measurements at great depths: implications for production rates by fast muons. Earth Planet. Sci. Lett. 211, 251–258. https://doi.org/10.1016/S0012-821X(03)00205-X.

Braucher, R., Merchel, S., Borgomano, J., Bourlès, D.L., 2011. Production of cosmogenic radionuclides at great depth: a multi element approach. Earth Planet. Sci. Lett. 309, 1–9. https://doi.org/10.1016/j.epsl.2011.06.036.

Brown, E.T., Stallard, R.F., Larsen, M.C., Raisbeck, G.M., Yiou, F., 1995. Denudation rates determined from the accumulation of in situ-produced10Be in the luquillo experimental forest, Puerto Rico. Earth Planet. Sci. Lett. https://doi.org/10.1016/0012-821X(94)00249-X.

Charreau, J., Blard, P.H., Puchol, N., Avouac, J.P., Lallier-Vergès, E., Bourlès, D., Braucher, R., Gallaud, A., Finkel, R., Jolivet, M., Chen, Y., Roy, P., 2011. Paleo-erosion rates in Central Asia since 9Ma: a transient increase at the onset of Quaternary glaciations? Earth Planet. Sci. Lett. 304, 85–92. https://doi.org/10.1016/j.epsl.2011.01.018.

Chmeleff, J., von Blanckenburg, F., Kossert, K., Jakob, D., 2010. Determination of the10Be half-life by multicollector ICP-MS and liquid scintillation counting. Nucl. Instrum. Methods Phys. Res. Sect. B Beam Interact. Mater. Atomos. https://doi.org/10.1016/j.nimb.2009.09.012.

Collins, D.B.G., 2004. Modeling the effects of vegetation-erosion coupling on landscape evolution. J. Geophys. Res. 109, 1–11. https://doi.org/10.1029/2003JF000028.

D'Arcy, M., Roda-boluda, D., Whittaker, A., 2017. Glacial-interglacial climate changes recorded by debris flow fan deposits, Owens Valley, California. Quat. Sci. Rev. 169, 288–311. https://doi.org/10.1016/j.quascirev.2017.06.002.

Dixon, J.L., Riebe, C.S., 2014. Tracing and pacing soil across slopes. Elements. https://doi.org/10.2113/gselements.10.5.363.

Ferrier, K.L., Huppert, K.L., Perron, J.T., 2013. Climatic control of bedrock river incision. Nature 496, 206–209. https://doi.org/10.1038/nature11982.

Fülöp, R.H., Bishop, P., Fabel, D., Cook, G.T., Everest, J., Schnabel, C., Codilean, A.T., Xu, S., 2015. Quantifying soil loss with in-situ cosmogenic10Be and14C depth-profiles. Quat. Geochronol. 27, 78–93. https://doi.org/10.1016/j.quageo.2015.01.003.

Garcin, Y., Schildgen, T.F., Torres Acosta, V., Melnick, D., Guillemoteau, J., Willenbring, J., Strecker, M.R., 2017. Short-lived increase in erosion during the African humid period: evidence from the northern Kenya rift. Earth Planet. Sci. Lett. 459, 58–69. https://doi.org/10.1016/j.epsl.2016.11.017.

Gosse, J.C., Phillips, F.M., 2001. Terrestrial in situ cosmogenic nuclides: theory and application. Quat. Sci. Rev. 20, 1475–1560. https://doi.org/10.1016/S0277-3791(00)00171-2.

Granger, D.E., Kirchner, J.W., Finkel, R., 1996. Spatially averaged long-term erosion rates measured from in situ-produced cosmogenic nuclides in alluvial sediment. J. Geol. 104, 249–257. https://doi.org/10.1086/629823.

Granger, D.E., Lifton, N.A., Willenbring, J.K., 2013. A cosmic trip: 25 years of cosmogenic nuclides in geology. Bull. Geol. Soc. Am. 125. https://doi.org/10.1130/B30774.1.

Granger, D.E., Riebe, C.S., 2013. Cosmogenic nuclides in weathering and erosion. In: Treatise on Geochemistry, second ed. . https://doi.org/10.1016/B978-0-08-095975-7.00514-3.

Grischott, R., Kober, F., Lupker, M., Reitner, J.M., Drescher-Schneider, R., Hajdas, I., Christl, M., Willett, S.D., 2017. Millennial scale variability of denudation rates for the last 15 kyr inferred from the detrital10Be record of lake Stappitz in the Hohe Tauern Massif, Austrian Alps. Holocene 27, 1914–1927. https://doi.org/10.1177/0959683617708451.

Hales, T.C., Roering, J.J., 2007. Climatic controls on frost cracking and implications for the evolution of bedrock landscapes. J. Geophys. Res. Earth Surf. 112, 1–14. https://doi.org/10.1029/2006JF000616.

Heisinger, B., Lal, D., Jull, A.J.T., Kubik, P., Ivy-Ochs, S., Knie, K., Nolte, E., 2002a. Production of selected cosmogenic radionuclides by muons: 2. Capture of negative muons. Earth Planet. Sci. Lett. 200, 357–369. https://doi.org/10.1016/S0012-821X(02)00641-6.

Heisinger, B., Lal, D., Jull, A.J.T., Kubik, P., Ivy-Ochs, S., Neumaier, S., Knie, K., Lazarev, V., Nolte, E., 2002b. Production of selected cosmogenic radionuclides by muons 1. Fast muons. Earth Planet. Sci. Lett. 200, 345–355. https://doi.org/10.1016/S0012-821X(02)00640-4.

Hidy, A.J., Gosse, J.C., Blum, M.D., Gibling, M.R., 2014. Glacial-interglacial variation in denudation rates from interior Texas, USA, established with cosmogenic nuclides. Earth Planet. Sci. Lett. 390, 209–221. https://doi.org/10.1016/j.epsl.2014.01.011.

Hippe, K., 2017. Constraining processes of landscape change with combined in situ cosmogenic 14 C- 10 Be analysis. Quat. Sci. Rev. 173, 1–19. https://doi.org/10.1016/j.quascirev.2017.07.020.

Hippe, K., Kober, F., Zeilinger, G., Ivy-Ochs, S., Maden, C., Wacker, L., Kubik, P.W., Wieler, R., 2012. Quantifying denudation rates and sediment storage on the eastern Altiplano, Bolivia, using cosmogenic 10Be, 26Al, and in situ 14C. Geomorphology 179, 58–70. https://doi.org/10.1016/j.geomorph.2012.07.031.

Jerolmack, D.J., Paola, C., 2010. Shredding of environmental signals by sediment transport. Geophys. Res. Lett. https://doi.org/10.1029/2010GL044638.

Knudsen, M.F., Egholm, D.L., 2018. Constraining Quaternary ice covers and erosion rates using cosmogenic 26Al/10Be nuclide concentrations. Quat. Sci. Rev. 181, 65–75. https://doi.org/10.1016/j.quascirev.2017.12.012.

Korschinek, G., Bergmaier, A., Faestermann, T., Gerstmann, U.C., Knie, K., Rugel, G., Wallner, A., Dillmann, I., Dollinger, G., von Gostomski, C.L., Kossert, K., Maiti, M., Poutivtsev, M., Remmert, A., 2010. A new value for the half-life of10Be by Heavy-Ion Elastic Recoil Detection and liquid scintillation counting. Nucl. Instrum. Methods Phys. Res. Sect. B Beam Interact. Mater. Atomos. https://doi.org/10.1016/j.nimb.2009.09.020.

Lal, D., 1991. Cosmic ray labeling of erosion surfaces: in situ nuclide production rates and erosion models. Earth Planet. Sci. Lett. 104, 424–439. https://doi.org/10.1016/0012-821X(91)90220-C.

Langbein, W.B., Schumm, S.A., 1958. Yield of sediment in relation to mean annual precipitation. Eos, Trans. Am. Geophys. Union 39, 1076–1084. https://doi.org/10.1029/TR039i006p01076.

Lisiecki, L.E., Raymo, M.E., 2005. A Pliocene-Pleistocene stack of 57 globally distributed benthic d18O records. Paleoceanography 20, 1–17. https://doi.org/10.1029/2004PA001071.

Lupker, M., Hippe, K., Wacker, L., Kober, F., Maden, C., Braucher, R., Bourlès, D., Romani, J.R.V., Wieler, R., 2015. Depth-dependence of the production rate of in situ^{14}C in quartz from the Leymon High core, Spain. Quat. Geochronol. 28, 80–87. https://doi.org/10.1016/j.quageo.2015.04.004.

Marrero, S.M., Phillips, F.M., Borchers, B., Lifton, N., Aumer, R., Balco, G., 2016. Cosmogenic nuclide systematics and the CRONUScalc program. Quat. Geochronol. 31, 160–187. https://doi.org/10.1016/j.quageo.2015.09.005.

Marshall, J.A., Roering, J.J., Bartlein, P.J., Gavin, D.G., Granger, D.E., Rempel, A.W., Praskievicz, S.J., Hales, T.C., 2015. Frost for the trees: did climate increase erosion in unglaciated landscapes during the late Pleistocene? Sci. Adv. 1 e1500715–e1500715. https://doi.org/10.1126/sciadv.1500715.

Milliman, J.D., Syvitski, J.P.M., 1992. Geomorphic/tectonic control of sediment discharge to the ocean: the importance of small Mountainous rivers. J. Geol. 100, 525–544. https://doi.org/10.1086/629606.

Montgomery, D.R., 2007. Soil erosion and agricultural sustainability. Proc. Natl. Acad. Sci. https://doi.org/10.1073/pnas.0611508104.

Mudd, S.M., 2017. Detection of transience in eroding landscapes. Earth Surf. Process. Landforms 42, 24–41. https://doi.org/10.1002/esp.3923.

Niemi, N.A., Oskin, M., Burbank, D.W., Heimsath, A.M., Gabet, E.J., 2005. Effects of bedrock landslides on cosmogenically determined erosion rates. Earth Planet. Sci. Lett. 237, 480–498. https://doi.org/10.1016/j.epsl.2005.07.009.

Nishiizumi, K., 2004. Preparation of 26Al AMS standards. Nucl. Instrum. Methods Phys. Res. Sect. B Beam Interact. Mater. Atomos. 223–224, 388–392. https://doi.org/10.1016/j.nimb.2004.04.075.

Phillips, F.M., Argento, D.C., Balco, G., Caffee, M.W., Clem, J., Dunai, T.J., Finkel, R., Goehring, B., Gosse, J.C., Hudson, A.M., Jull, A.J.T., Kelly, M.A., Kurz, M., Lal, D., Lifton, N., Marrero, S.M., Nishiizumi, K., Reedy, R.C., Schaefer, J., Stone, J.O.H., Swanson, T., Zreda, M.G., 2016. The CRONUS-Earth Project: a synthesis. Quat. Geochronol. 31, 119–154. https://doi.org/10.1016/j.quageo.2015.09.006.

Riebe, C.S., Granger, D.E., 2013. Quantifying effects of deep and near-surface chemical erosion on cosmogenic nuclides in soils, saprolite, and sediment. Earth Surf. Process. Landforms 38, 523–533. https://doi.org/10.1002/esp.3339.

Roering, J.J., Almond, P., Tonkin, P., McKean, J., 2004. Constraining climatic controls on hillslope dynamics using a coupled model for the transport of soil and tracers: application to loess-mantled hillslopes, South Island, New Zealand. J. Geophys. Res. 109, 1–19. https://doi.org/10.1029/2003JF000034.

Schaller, M., Ehlers, T.A., 2006. Limits to quantifying climate driven changes in denudation rates with cosmogenic radionuclides. Earth Planet. Sci. Lett. 248, 138–152. https://doi.org/10.1016/j.epsl.2006.05.027.

Schaller, M., von Blanckenburg, F., Hovius, N., Kubik, P.W., 2001. Large scale erosion rates from in situ produced cosmogenic nuclides in European river sediments. Earth Planet. Sci. Lett. 188, 441–458.

Schaller, M., Von Blanckenburg, F., Veldkamp, A., Tebbens, L.A., Hovius, N., Kubik, P.W., 2002. A 30 000 yr record of erosion rates from cosmogenic 10Be in Middle European river terraces. Earth Planet. Sci. Lett. 204, 307–320. https://doi.org/10.1016/S0012-821X(02)00951-2.

Small, E.E., Anderson, R.S., Repka, J.L., Finkel, R.C., 1997. Erosion rates of alpine bedrock summit surfaces deduced from in situ 10Be and 26Al. Earth Planet. Sci. Lett. 150, 413–425. https://doi.org/10.1016/S0012-821X(97)00092-7.

Syvitski, J.P.M., 2003. Supply and flux of sediment along hydrological pathways: Research for the 21st century. Glob. Planet. Change 39, 1–11. https://doi.org/10.1016/S0921-8181(03)00008-0.

von Blanckenburg, F., 2006. The control mechanisms of erosion and weathering at basin scale from cosmogenic nuclides in river sediment. Earth Planet. Sci. Lett. 242, 224–239. https://doi.org/10.1016/j.epsl.2005.11.017.

Whipple, K.X., 2001. Fluvial landscape response time: how plausible is steady-state denudation? Am. J. Sci. 301, 313–325. https://doi.org/10.2475/ajs.301.4-5.313.

Yanites, B.J., Tucker, G.E., Anderson, R.S., 2009. Numerical and analytical models of cosmogenic radionuclide dynamics in landslide-dominated drainage basins. J. Geophys. Res. Earth Surf. 114. https://doi.org/10.1029/2008JF001088.